Quasi-analytical treatment of spatially averaged radiation transfer in complex terrain

H. Löwe[1] and N. Helbig[2]

Received 24 May 2012; revised 17 August 2012; accepted 21 August 2012; published 2 October 2012.

[1] We provide a new quasi-analytical method to compute the subgrid topographic influences on the shortwave radiation fluxes and the effective albedo in complex terrain as required for large-scale meteorological, land surface, or climate models. We investigate radiative transfer in complex terrain via the radiosity equation on isotropic Gaussian random fields. Under controlled approximations we derive expressions for domain-averaged fluxes of direct, diffuse, and terrain radiation and the sky view factor. Domain-averaged quantities can be related to a type of level-crossing probability of the random field, which is approximated by long-standing results developed for acoustic scattering at ocean boundaries. This allows us to express all nonlocal horizon effects in terms of a local terrain parameter, namely, the mean-square slope. Emerging integrals are computed numerically, and fit formulas are given for practical purposes. As an implication of our approach, we provide an expression for the effective albedo of complex terrain in terms of the Sun elevation angle, mean-square slope, the area-averaged surface albedo, and the ratio of atmospheric direct beam to diffuse radiation. For demonstration we compute the decrease of the effective albedo relative to the area-averaged albedo in Switzerland for idealized snow-covered and clear-sky conditions at noon in winter. We find an average decrease of 5.8% and spatial patterns which originate from characteristics of the underlying relief. Limitations and possible generalizations of the method are discussed.

Citation: Löwe, H., and N. Helbig (2012), Quasi-analytical treatment of spatially averaged radiation transfer in complex terrain, *J. Geophys. Res.*, *117*, D19101, doi:10.1029/2012JD018181.

1. Introduction

[2] The importance of including terrain effects into the shortwave radiation balance in complex terrain has been widely known for a long time [*Dozier and Outcalt*, 1979]. Local incoming fluxes might be strongly reduced at locations which are shadowed by remote terrain or might be significantly enhanced at locations which receive additional reflected radiation from adjacent terrain. The latter effect is particularly important for snow-covered areas where surface albedos are high. As a result, terrain effects generally increase spatial heterogeneities of local incoming fluxes when compared to flat surfaces. But also spatially averaged values of incoming and reflected fluxes change due to the presence of terrain. As addressed in *Weihs et al.* [2000] for UV radiation, the so-called effective albedo of a large mountainous domain is lower than a simple area average of the surface albedo. Similar terrain effects on the albedo must be taken into account for remote sensing application [*Wen et al.*, 2009]. The notion of an effective albedo has important consequences for coarse-resolution meteorological, land surface, or climate models which do not fully resolve the topography and resort to so-called subgrid parametrizations to include terrain effects. The impact of resolved topography on radiation transfer in numerical weather prediction has been recently addressed by *Manners et al.* [2012] for the Met Office Unified Model. In particular for snow cover processes in mountainous terrain, as a sensitive indicator for climate change, subgrid topography increases the model efficiency of large-scale models [*Parajka et al.*, 2010].

[3] The impact of terrain effects on the radiation balance is certainly best investigated by photon tracing simulations [*Chen et al.*, 2006; *Liou et al.*, 2007]. A recent application of the Monte Carlo approach specifically highlighted its relevance for applications in climate modeling [*Lee et al.*, 2011]. However, the computational complexity of these methods still prevents their direct incorporation into large-scale models [*Lee et al.*, 2011] and the analysis of Monte Carlo simulations must eventually resort to empirical regressions to relate topographic parameters to simulated fluxes. To connect sophisticated simulations to simple subgrid parametrizations it would be desirable to aim at simplified model systems of radiation transfer in complex terrain, yielding simple, analytical parametrization formulas which guide the development of parametrization schemes.

[1]WSL Institute for Snow and Avalanche Research SLF, Davos, Switzerland.
[2]Department of Civil Engineering, Montana State University Bozeman, Montana, USA.

Corresponding author: H. Löwe, WSL Institute for Snow and Avalanche Research SLF, Flüelastr. 11, CH-7260 Davos, Switzerland. (loewe@slf.ch)

0148-0227/12/2012JD018181

[4] On a semiempirical level a large number of studies has been hitherto devoted to the parametrization of terrain effects in complex topography [*Dozier and Frew*, 1990; *Dubayah et al.*, 1990; *Olyphant*, 1986; *Müller and Scherer*, 2005; *Essery and Marks*, 2007]. Most of them include shadowing and limited sky view as the most important geometric influences of the topography. However, shadowing and limited sky view must be computed from the horizon line, an inherent nonlocal quantity. Since horizons cannot be computed from nearest neighbor heights of the underlying digital height model (DHM), the incorporation of shadowing is less straightforward. For some parametrizations the degree of simplification remains unclear and their relation to Monte Carlo approaches can barely be put on firm theoretical grounds. Toward a remedy *Helbig et al.* [2009] have derived the radiosity approach under controlled simplifications from generic radiative transfer in complex terrain. It can be shown that the radiosity approach compares reasonably well to Monte Carlo simulations for point measurements [*Helbig et al.*, 2010] for clear sky days. On the other hand domain averages within the radiosity approach compare well to a parametrization developed in *Helbig and Löwe* [2012] which is based on the sky view factor and the parametrization by *Dubayah et al.* [1990] for the direct flux. The validation has been carried out for Gaussian random fields as model topographies which could be shown to capture relevant geometrical aspects of realistic complex terrain [*Helbig and Löwe*, 2012]. However, the parametrization of [*Dubayah et al.*, 1990] and likewise [*Helbig and Löwe*, 2012] do not include partial shading of the terrain by remote topography for low Sun elevations. In addition the sky view factor is explicitly contained as a parameter which must be determined in advance.

[5] In this paper we present a new, quasi-analytical method to derive parametrizations for all radiation components and the sky view factor in complex terrain from the radiosity equation on Gaussian random fields. By accepting the underlying simplifications in the first place we can make significant progress from a well-defined mathematical framework. To this end we show how the effective albedo, as required for coarse resolution models, originates from geometrical properties of the topography in a high-resolution model. Thereby domain-averaged radiation fluxes can be solely expressed in terms of slope characteristics, i.e., local quantities. This essential step is accomplished by relating domain-averaged fluxes in complex terrain to a type of level-crossing probability of the topographic surface. Thereby nonlocal horizon effects, namely, sky view factor and shadowing are treated implicitly and related to integrals over the level-crossing probability. This constitutes a main difference to [*Essery and Marks*, 2007] where the horizon must be computed explicitly from the DHM. By using long-standing results put forward for acoustic scattering from sea surfaces we are able to compute the integrals numerically. This enables us to derive practical formulas for the radiation components and the effective albedo solely in terms of the mean-square slope. These parametrizations include partial shading of the terrain for low Sun elevations close to sunset. Our results enable a straightforward application in large-scale models by efficient DHM preprocessing without prior computation of sky view factors. This is demonstrated by computing the effective albedo for the entire Swiss Alps.

[6] Our method requires that the grid size of the coarse model is sufficiently large compared to the correlation length of the subgrid topography. Additionally, by using the radiosity approach as presently formulated in *Helbig et al.* [2009] we neglect atmospheric effects and thus focus on the influence of topography under clear sky conditions. Similar to [*Lee et al.*, 2011] we assume however that our results provide a reasonable first-order estimate for the shortwave fluxes. Some limitations of our approach can however be overcome with existing generalizations of the present level-crossing framework.

2. Theory

2.1. Subgrid Topography and Coordinate Systems

[7] We consider a part of complex terrain as schematically shown in Figure 1: The topography is given as a surface A from a high-resolution DHM with fine grid size Δx. The enclosing three-dimensional box in Figure 1 can be envisaged as a surface grid box of a large-scale (land surface, meteorological, or climate) model with coarse grid size L. On the coarse grid the topography is not fully resolved and solely represented by the flat (red) surface $\widetilde{A}$. Without loss of generality we focus on the case where $\widetilde{A}$ has vanishing slope, the results can be easily extended to the case where $\widetilde{A}$ has nonvanishing slope as demonstrated later. The topography is illuminated by the Sun at elevation angle θ_e. We assume that L is not too coarse so that the Sun azimuth and elevation can be regarded as constant for all locations on $\widetilde{A}$. In addition we assume that the surface A has an arbitrary surface albedo $\alpha(x)$ which may depend on position but is uncorrelated with topographic features. This might be unrealistic for particular snow cover situations, e.g., for ablation where high albedo values can only be found for particular slopes and elevations. A remedy is outlined in the discussion. In the following the area-averaged surface albedo is denoted by $\langle\alpha\rangle$.

[8] We assume that the large-scale model on the coarse grid provides values S_b, S_d of bare downwelling direct beam and isotropic diffuse fluxes, respectively, which are left unspecified henceforth. On the coarse grid the surface $\widetilde{A}$ receives a global incoming flux

$$\widetilde{S}_{sky} = S_b \sin\theta_e + S_d. \tag{1}$$

The simplest estimate $S_g^{out} = \langle\alpha\rangle\widetilde{S}_{sky}$ for the global outgoing radiation would employ the area-averaged surface albedo which appears to be wrong [*Weihs et al.*, 2000]. By computing the radiative interaction of the bare fluxes S_b, S_d with the topographic surface A we shall show below how an effective albedo α_{eff} can be defined for the surface $\widetilde{A}$ such that the true outgoing flux $S_g^{out} = \alpha_{eff}\widetilde{S}_{sky}$ is obtained.

[9] For convenience we orient the x axis of the horizontal coordinate system in the Sun azimuth direction such that the Sun vector given by $\boldsymbol{r}_s = (\cos(\theta_e), 0, \sin(\theta_e))$. In the x, z plane we define angles and slopes as indicated in Figure 2. Partial derivatives of the height are denoted by $m_x := \partial h/\partial x$, $m_y := \partial h/\partial y$ and related to the slope angle ζ via $\tan^2(\zeta) = m_x^2 + m_y^2$. The Sun slope $m_e = \tan(\theta_e)$ and the horizon slope $m_h := \tan(\theta_h)$ which are defined at a position $\boldsymbol{x}$ on A in the *horizontal* coordinate system are denoted by lowercase symbols. In addition

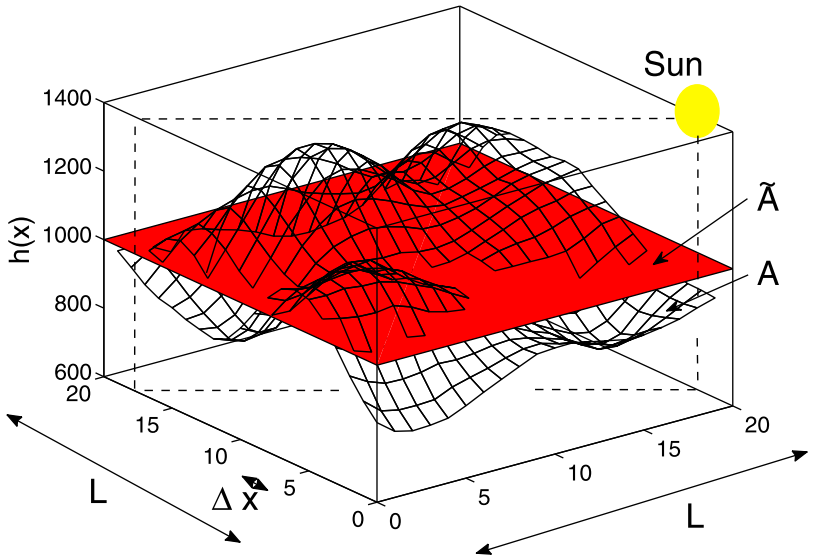

Figure 1. Schematic of a flat grid cell $\widetilde{A}$ with coarse resolution L and the subgrid topography represented by a surface A on a fine grid with resolution Δx.

we need the respective horizon slope $M_h = \tan(\Theta_h)$ at the point $\boldsymbol{x}$ in the sloped (tangent plane) coordinate system which is denoted by an upper case symbol. The surface normal vector $\boldsymbol{n} = \left(-m_x, -m_y, 1\right)/\sqrt{1 + m_x^2 + m_y^2}$ constitutes the local $\boldsymbol{e}_z$ axis in the sloped system. Though completely equivalent, we formulate the theory wherever possible in terms of slopes (m_e, m_h, m_x, m_y), rather than angles $(\theta_e, \theta_h, \zeta)$, which simplifies matters.

2.2. Gaussian Random Fields

[10] To explicitly include complex terrain in the model we treat the topographic height $h(\boldsymbol{x})$ for $\boldsymbol{x} \in \mathbb{R}^2$ as an isotropic, stationary Gaussian random field with zero mean and covariance

$$C(|\boldsymbol{r}|) = \overline{h(\boldsymbol{x})h(\boldsymbol{x}+\boldsymbol{r})} = \sigma^2 \exp\left(-(|\boldsymbol{r}|/\xi)^2\right). \qquad (2)$$

Here σ denotes the variance of the surface height and ξ is a correlation length, characterizing typical heights and widths of topographic features respectively. Ensemble averages over the field are denoted by $\bar{\bullet}$. Due to isotropy the covariance (2) depends only on the magnitude of the lag vector $\boldsymbol{r}$. We have previously shown [*Helbig and Löwe*, 2012] that deviations from isotropy are rather small for various real mountain domains from the US and Swiss Alps

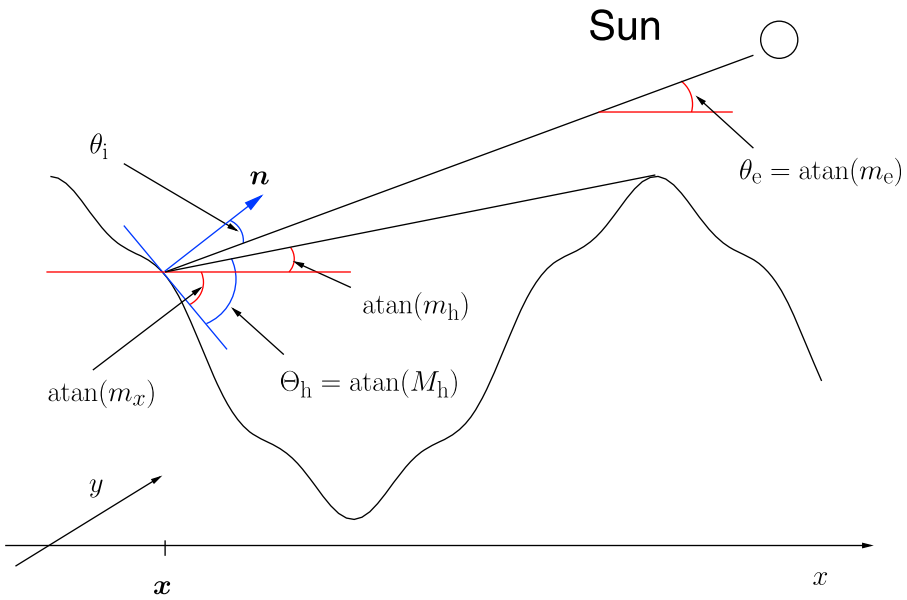

Figure 2. Notation for the geometry on the intersect of the surface A with the Sun plane (indicated by dashed lines in Figure 1).

for grid sizes within 2.5 km < L < 6.5 km. Isotropic fields should therefore serve as a simple but reasonable starting point.

[11] For later convenience we note that the covariance (2) implies a joint probability density

$$p_s(m_x, m_y) = \frac{1}{2\pi\mu^2} \exp\left(-\frac{m_x^2 + m_y^2}{2\mu^2}\right) \tag{3}$$

for the partial derivatives m_x, m_y. Due to isotropy the joint density factorizes into two Gaussians with zero mean and standard deviation $\mu = \sqrt{2}\sigma/\xi$ which constitutes the key parameter of the subsequent analysis. Alternatively, the parameter μ can be related to the mean-square slope via

$$2\mu^2 = \overline{m_x^2 + m_y^2} = \overline{\tan^2(\zeta)}. \tag{4}$$

2.3. Sky Radiation

[12] Unlike the incoming flux (1) on the flat surface $\widetilde{A}$, the incoming direct beam and diffuse components on A depend on spatial position

$$S_{\mathrm{sky}}(\boldsymbol{x}) = S_b\, \lambda(\theta_e, \boldsymbol{x}) + S_d F_{\mathrm{sky}}(\boldsymbol{x}) \tag{5}$$

due to slope variations, shadowing and limited sky view. The spatial dependence of direct beam radiation in (5) is subsumed in the geometric quantity

$$\lambda(\theta_e, \boldsymbol{x}) := \cos(\theta_i(\boldsymbol{x}))\, H(m_e - m_h(\boldsymbol{x})) \tag{6}$$

which includes the local incidence angle $\cos(\theta_i) = \boldsymbol{n} \cdot \boldsymbol{r}_s$ and shadowing via the Heaviside function $H(x)$, with $H(x) = 1$ for $x > 0$ and $H(x) = 0$ for $x < 0$. This conveniently implements the requirement that the horizon angle must be smaller than the Sun angle to receive direct beam radiation. Using equation (1.624.7/8) in *Gradshteyn and Ryzhik* [2000] the incidence angle can be rewritten in terms of slopes according to

$$\cos(\theta_i) = \frac{m_e - m_x}{\left[\left(1 + m_e^2\right)\left(1 + m_x^2 + m_y^2\right)\right]^{1/2}}. \tag{7}$$

[13] The spatial dependence of the diffuse component in (5) stems from the sky view factor $F_{\mathrm{sky}}(\boldsymbol{x})$. As shown in [*Helbig et al.*, 2009], the sky view factor can be written as

$$F_{\mathrm{sky}}(\boldsymbol{x}) = \frac{1}{2\pi} \int_0^{2\pi} \mathrm{d}\Phi\, \cos^2(\Theta_h(\Phi)) \tag{8}$$

in terms of the horizon angles $\Theta_h(\Phi) = \arctan(M_h(\Phi))$ in azimuth direction Φ in the sloped coordinate system. According to Figure 1, angles are counted positive in counterclockwise direction relative to the respective x axis and thus sum up according to $\arctan(M_h) = \arctan(m_h) - \arctan(m_x)$. This can be rewritten by virtue of equation (1.313.9) in *Gradshteyn and Ryzhik* [2000], and yields a relation

$$M_h = \frac{m_h - m_x}{1 + m_h m_x} \tag{9}$$

between the horizons in the horizontal system and the sloped system. Equation (9) reveals that computing the sky view factor from the horizon line in the horizontal system is strictly wrong and might be used only for very flat terrain $m_x \approx 0$, where equation (9) yields $M_h \approx m_h$. This is often ignored in literature.

2.4. Global Incoming Radiation and Radiosity Equation

[14] In addition to the sky fluxes (5), radiation is also received from remote terrain by reflections. As previously shown in *Helbig et al.* [2010] the influence of terrain under clear sky conditions can be well described by the radiosity approach [*Helbig et al.*, 2009]. The global incoming radiation $S_g(\boldsymbol{x})$ at $\boldsymbol{x}$ is the solution of the radiosity integral equation

$$S_g(\boldsymbol{x}) = S_{\mathrm{sky}}(\boldsymbol{x}) + \int_A dA\, K(\boldsymbol{x}, \boldsymbol{x}')\alpha(\boldsymbol{x}')S_g(\boldsymbol{x}'). \tag{10}$$

The precise form of the integral kernel $K(\boldsymbol{x}, \boldsymbol{x}')$ can be found in *Helbig et al.* [2009], which contains the mutual "view factors." That precise form is however not of importance here, we only need a normalization property, namely, that the sky view factor (8) is related to the integral kernel via

$$F_{\mathrm{sky}}(\boldsymbol{x}) = 1 - \int_A dA K(\boldsymbol{x}, \boldsymbol{x}'). \tag{11}$$

Note that the integral in equation (10) is a surface integral over A and the radiosity equation (10) is a Fredholm integral equation of the second kind [*Atkinson*, 2006] which can be formally solved analytically in terms of a von Neumann series. Such a perturbative solution is also common to other problems of radiative transfer which involve integral equations [see, e.g., *Marshak and Davis*, 2005]. Here we keep only the linear order term which corresponds to the single-reflection approximation. The solution thus reads

$$S_g(\boldsymbol{x}) = S_{\mathrm{sky}}(\boldsymbol{x}) + \int_A dA\, K(\boldsymbol{x}, \boldsymbol{x}')\alpha(\boldsymbol{x}')S_{\mathrm{sky}}(\boldsymbol{x}'). \tag{12}$$

The first-order approximation becomes increasingly poor if the norm of the integral kernel approaches unity, which is for $\alpha \to 1$ and $F_{\mathrm{sky}} \to 0$, i.e., for perfectly reflecting surfaces in infinitely steep topographies. The second term in equation (12) can be identified with the terrain radiation

$$S_{\mathrm{ter}}(\boldsymbol{x}) := \int_A dA\, K(\boldsymbol{x}, \boldsymbol{x}')\alpha(\boldsymbol{x}')S_{\mathrm{sky}}(\boldsymbol{x}') \tag{13}$$

yielding $S_g(\boldsymbol{x}) = S_{\mathrm{sky}}(\boldsymbol{x}) + S_{\mathrm{ter}}(\boldsymbol{x})$.

2.5. Averages Over the Random Field

[15] Now we are interested in averages over the random field to compute the averaged global flux $\overline{S_g(\boldsymbol{x})}$. This requires averaging the product $\overline{K(\boldsymbol{x}, \boldsymbol{x}')\alpha(\boldsymbol{x}')S_{\mathrm{sky}}(\boldsymbol{x}')}$ in equation (12). First, we carry out the area-averaged $\langle\alpha\rangle$ of the albedo which has been assumed to be independent of the random field, yielding $\langle\alpha\rangle\overline{K(\boldsymbol{x}, \boldsymbol{x}')S_{\mathrm{sky}}(\boldsymbol{x}')}$. To make analytical progress we approximate the average of the product (which would require two-point statistics) by a product of averages, i.e., by one-point statistics. This corresponds to a

mean field approach which neglects anisotropic effects of terrain radiation. These effects play a role if adjacent terrain is already shadowed, thereby receiving and reflecting less direct radiation than nonshadowed adjacent terrain [*Helbig et al.*, 2009; *Lee et al.*, 2011]. By virtue of (11) we end up with the averages of the two geometrical quantities $\overline{F_{\mathrm{sky}}(\boldsymbol{x})}$ and $\overline{\lambda(\theta_{\mathrm{e}},\boldsymbol{x})}$ over the random field. Due to stationarity of the field these averages do not depend on position and we end up with

$$\overline{S_{\mathrm{g}}}(\theta_{\mathrm{e}},\mu)=\left[1+\langle\alpha\rangle\left(1-\overline{F}_{\mathrm{sky}}(\mu)\right)\right]\left[S_{\mathrm{b}}\overline{\lambda}(\theta_{\mathrm{e}},\mu)\;+\;S_{\mathrm{d}}\overline{F}_{\mathrm{sky}}(\mu)\right] \tag{14}$$

where we made the dependence on the remaining parameters in $\overline{\lambda}(\theta_{\mathrm{e}},\mu):=\overline{\lambda(\theta_{\mathrm{e}},\boldsymbol{x})}$ and $\overline{F}_{\mathrm{sky}}(\mu):=\overline{F_{\mathrm{sky}}(\boldsymbol{x})}$ explicit.

[16] The domain-averaged direct beam term (6) is rewritten by equation (7) as

$$\overline{\lambda}(\theta_{\mathrm{e}},\mu)=\overline{\frac{m_{\mathrm{e}}-m_{\boldsymbol{x}}}{\left(\left(1+m_{\mathrm{e}}^2\right)\left(1+m_{\boldsymbol{x}}^2+m_y^2\right)\right)^{1/2}}H(m_{\mathrm{e}}-m_{\mathrm{h}})} \tag{15}$$

From equation (15) we can immediately derive an important result if the Sun is in zenith, i.e., $\theta_{\mathrm{e}}\to\pi/2$ or equivalently $m_{\mathrm{e}}\to\infty$ for which the Heaviside term equals unity. In this case equation (15) reduces to

$$\overline{\lambda}(\pi/2,\mu)=\overline{\left(1+m_{\boldsymbol{x}}^2+m_y^2\right)^{-1/2}}=\overline{\cos(\zeta)}. \tag{16}$$

The second equality stems from $\tan^2(\zeta)=m_x^2+m_y^2$ and equation (1.624.8) in *Gradshteyn and Ryzhik* [2000]. The average (16) can be computed exactly by integrating over the probability density (3) in polar coordinates and employing equation (3.362.2) in *Gradshteyn and Ryzhik* [2000]. This yields

$$\overline{\lambda}(\pi/2,\mu):=\sqrt{\frac{\pi}{2\mu^2}}\exp\left(\frac{1}{2\mu^2}\right)\mathrm{erfc}\left(1/\sqrt{2\mu^2}\right) \tag{17}$$

in terms of the complementary error function $\mathrm{erfc}(x)$. This result is later used as an independent test for our methodology. We note that equation (17) is the exact result for the averaged direct radiation if the Sun is in zenith. The result is different from the parametrization given in *Dubayah et al.* [1990] which uses $\cos\left(\overline{\zeta}\right)$. The difference lies in the order of averaging and application of the cosine. The correct order is to average over the cosine of the slope angle rather than computing the cosine of the averaged slope angle.

[17] For the average sky view factor in (14) we need to compute the average $\overline{\cos^2(\Theta_{\mathrm{h}}(\Phi))}$ in equation (8). Due to isotropy of the random field the average does not depend on the azimuth Φ. We thus choose $\Phi=0$ and rewrite $\cos^2(\Theta_{\mathrm{h}}(0))=\cos^2(\arctan M_{\mathrm{h}})=(1+M_{\mathrm{h}})^{-2}$ by using equation (1.624.8) in *Gradshteyn and Ryzhik* [2000]. Employing the relation (9) we can express the domain-averaged sky view factor as

$$\overline{F}_{\mathrm{sky}}(\mu)=\overline{\frac{\left(1+m_{\boldsymbol{x}}m_{\mathrm{h}}\right)^2}{\left(1+m_{\boldsymbol{x}}^2\right)\left(1+m_{\mathrm{h}}^2\right)}} \tag{18}$$

in terms of the local slope m_x in x direction and the tangent of the horizon angle in the horizontal coordinate system m_{h}. Isotropy allows us to express $\overline{F}_{\mathrm{sky}}(\mu)$ solely as a function of m_x.

2.6. Global Outgoing Radiation and the Effective Albedo

[18] The effective albedo of the large-scale model is now defined by

$$\alpha_{\mathrm{eff}}:=\frac{S_{\mathrm{g}}^{\mathrm{out}}}{\widetilde{S}_{\mathrm{sky}}}. \tag{19}$$

It relates the true global outgoing radiation $S_{\mathrm{g}}^{\mathrm{out}}$ which is reflected back from the surface A into the sky and the apparent incoming flux $\widetilde{S}_{\mathrm{sky}}$ on $\widetilde{A}$ from equation (1). If both fluxes are given per unit area of the flat cell $\widetilde{A}$, the definition (19) ensures that the large-scale model yields the correct flux.

[19] To compute the true global outgoing flux (per unit area of the flat cell $\widetilde{A}$) we integrate all contributions from the surface A which are reflected back to the sky and divide by the area of the flat cell $\widetilde{A}$, viz $S_{\mathrm{g}}^{\mathrm{out}}=L^{-2}\int_A dA F_{\mathrm{sky}}(\boldsymbol{x})\alpha(\boldsymbol{x})S_{\mathrm{g}}(\boldsymbol{x})$. The surface integral over A can be transformed into an integral over $\widetilde{A}$ via $\int_A dA=\int_{\widetilde{A}} d^2x\cos(\zeta(\boldsymbol{x}))^{-1}$ yielding

$$S_{\mathrm{g}}^{\mathrm{out}}=\frac{1}{L^2}\int_{\widetilde{A}} d^2x\cos(\zeta(\boldsymbol{x}))^{-1}F_{\mathrm{sky}}(\boldsymbol{x})\alpha(\boldsymbol{x})S_{\mathrm{g}}(\boldsymbol{x}). \tag{20}$$

Because our Gaussian random field is ergodic [*Adler*, 1981], ensemble averages can be obtained by spatial averaging via $\overline{f(\boldsymbol{x})}=\lim_{L\to\infty}L^{-2}\int_{\widetilde{A}} d^2x f(\boldsymbol{x})$. This requires L to be sufficiently large compared to the surface correlation length ξ in (2). As a first step we employ $L/\xi\to\infty$ for analytical tractability, in general one will expect corrections for finite values of L/ξ. The discussion of this point is postponed to the last section. In the limit of $L/\xi\to\infty$ the outgoing radiation (20) can be written as an ensemble average over the random field and inserted into (19)

$$\alpha_{\mathrm{eff}}(\theta_{\mathrm{e}},\mu)=\langle\alpha\rangle\frac{\overline{S_{\mathrm{g}}(\boldsymbol{x})F_{\mathrm{sky}}(\boldsymbol{x})\cos(\zeta(\boldsymbol{x}))^{-1}}}{S_{\mathrm{b}}\sin(\theta_{\mathrm{e}})+S_{\mathrm{d}}}. \tag{21}$$

In the following we further approximate equation (21) in terms of previously derived quantities. To this end we split the average of the product in the nominator into a product of averages, then replace $\overline{\cos(\zeta(\boldsymbol{x}))^{-1}}\approx\overline{\cos(\zeta(\boldsymbol{x}))}^{-1}$ which can be further rewritten in terms of $\overline{\cos(\zeta(\boldsymbol{x}))}=\overline{\lambda}(\pi/2,\mu)$ by virtue of equation (16). In addition we introduce the ratio of direct beam to diffuse radiation $\rho=S_{\mathrm{b}}/S_{\mathrm{d}}$ to obtain

$$\alpha_{\mathrm{eff}}(\theta_{\mathrm{e}},\mu,\rho,\langle\alpha\rangle)/\langle\alpha\rangle=\frac{\left[1+\langle\alpha\rangle\left(1-\overline{F}_{\mathrm{sky}}(\mu)\right)\right]\left[\rho\overline{\lambda}(\theta_{\mathrm{e}},\mu)+\overline{F}_{\mathrm{sky}}(\mu)\right]\overline{F}_{\mathrm{sky}}(\mu)}{\overline{\lambda}(\pi/2,\mu)[\rho\sin(\theta_{\mathrm{e}})+1]}. \tag{22}$$

In general the direct-to-diffuse ratio ρ is itself a function of Sun elevation θ_{e} [*Schmucki et al.*, 2001] and thus the effective

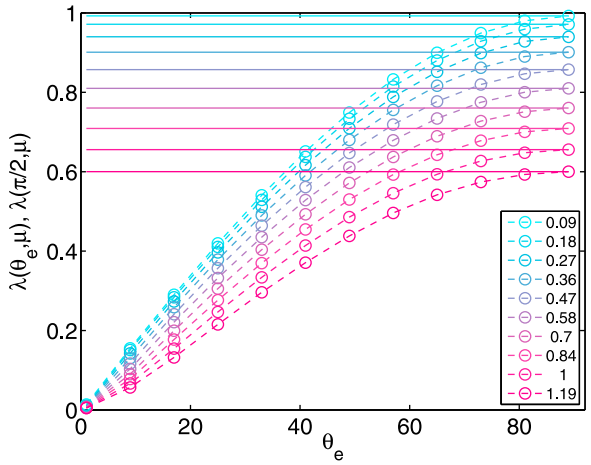

Figure 3. Domain-averaged direct beam radiation $\overline{\lambda}(\theta_e, \mu)$ as a function of Sun elevation angle for different values of μ (see legend). Horizontal lines show the required limiting behavior $\overline{\lambda}(\pi/2, \mu)$ from equation (17) which must be approached for $\theta_e \to \pi/2$.

albedo essentially becomes a function of only three independent variables $\alpha_{\mathrm{eff}}(\theta_e, \mu, \rho(\theta_e), \langle\alpha\rangle)$.

2.7. Relation to Level-Crossing Probabilities

[20] The remaining averages (15) and (18) which determine the averaged direct, diffuse and terrain radiation and thereby the effective albedo can be computed by integration with respect to the joint probability density $p(m_h, m_x, m_y)$ for the horizon and the slopes via

$$\overline{(\bullet)} = \int_{-\infty}^{\infty} \mathrm{d}m_x \int_{-\infty}^{\infty} \mathrm{d}m_y \int_{0}^{\infty} \mathrm{d}m_h (\bullet) p(m_h, m_x, m_y). \quad (23)$$

To proceed we rewrite the joint probability to apply long-standing results which have been derived in a different context. To this end we express the joint density in terms of a conditional density via $p(m_h, m_x, m_y) = p(m_h|m_x, m_y)\, p_s(m_x, m_y)$. In the present isotropic case the x and y direction are statistically independent and the horizon slope m_h in the x direction does not depend on m_y. This implies the simplification

$$p(m_h, m_x, m_y) = p(m_h|m_x) p_s(m_x, m_y). \quad (24)$$

Now we introduce the cumulative distribution function

$$\Phi(m_h|m_x) = \mathrm{Prob}(m_h(\boldsymbol{x}) < m_h \,|\, m_x(\boldsymbol{x}) \in [m_x, m_x + dm_x]) \quad (25)$$

of the conditional probability density $p(m_h|m_x)$ which denotes the probability that the horizon slope $m_h(\boldsymbol{x})$ is below a given value m_h (conditioned on the slope). In other words, (25) can be interpreted as the probability that the topography intersect in x direction does not cross the ray initiating from $\boldsymbol{x}$ on the surface A at slope m_h in x direction. It thus defines a particular type of level-crossing problem [*Adler*, 1981]. Likewise, it can be interpreted as the (conditional) probability that x is shadowed by distant terrain if the Sun is at elevation m_h [*Wagner*, 1967]. Since by definition $\Phi(m_h|m_x) = \int_{-\infty}^{m_h} dm_h' \, p(m_h'|m_x)$ we can rewrite (24) according to

$$p(m_h, m_x, m_y) = \left(\frac{\partial}{\partial m_h} \Phi(m_h|m_x)\right) p_s(m_x, m_y). \quad (26)$$

This is an exact representation of the probability density required to compute the domain averages (15) and (18) via (23). This constitutes the key result of our work since it shifts the problem of computing radiation components to the task of computing the level-crossing probability of the underlying topography. The level-crossing problem of Gaussian random surfaces cannot be solved exactly but many expressions of different degrees of rigor have been derived in various applications. In the following we use an approximation derived by *Wagner* [1967] to tackle scattering of sound waves from sea surfaces for Gaussian random fields. If correlations between slopes and heights are neglected the conditional distribution function (25) can be written as

$$\Phi(m_h|m_x) = H(m_h - m_x) \frac{1 - \exp\left[-2B\left(m_h/\sqrt{2\mu^2}\right)\right]}{2B\left(m_h/\sqrt{2\mu^2}\right)}$$
$$B(x) = \frac{\exp(-x^2) - \sqrt{\pi} x \,\mathrm{erfc}(x)}{2\sqrt{\pi} x} \quad (27)$$

where again $H(x)$ denotes the Heaviside step function, $\mathrm{erfc}(x)$ the complementary error function and $\mu = \sqrt{2}\sigma/\xi$ the standard deviation of the slope distribution. Here we point out that equation (22) in *Wagner* [1967] contains a typo: the 4 in the denominator for $B(x)$ has to be replaced by a 2 [cf. *Bourlier and Berginc*, 2003].

[21] It is noteworthy that limited sky view for the diffuse component and shadowing for the direct beam component can both be computed from the same probability density. This is not surprising since both are determined by the same geometrical quantity, namely, the horizon line.

[22] In the following we compute the averages (15), (18) via equation (23) and use (26) with the approximation (27) to carry out the integrals numerically. Note that Φ involves a Heaviside function which gives rise to a Dirac function in the derivative (26). We carry out the derivative in (26) analytically and integrate out the Dirac contribution prior to numerical treatment. We have used the symbolic algebra package MAPLE to calculate the integrals numerically.

3. Results

3.1. Domain-Averaged Incoming Direct Beam

[23] The domain-averaged direct beam radiation $\overline{\lambda}(\theta_e, \mu)$ is computed as a function of the Sun elevation angle $\theta_e = 1°, 9°, 17°, \ldots, 89°$ in Figure 3. The average is computed for different values of terrain steepness μ which are given in the legend. If these values for μ are translated into a typical slope angle via $\zeta = \mathrm{atan}\left(\sqrt{2}\mu\right)$ we cover a broad range of slope angles from $\zeta \approx 7°$ for $\mu = 0.09$ to $\zeta \approx 60°$ for $\mu = 1.19$. As an independent check for the averaging procedure via the level-crossing probability derived in the last section, we have plotted the limiting values $\overline{\lambda}(\pi/2, \mu)$ as horizontal lines,

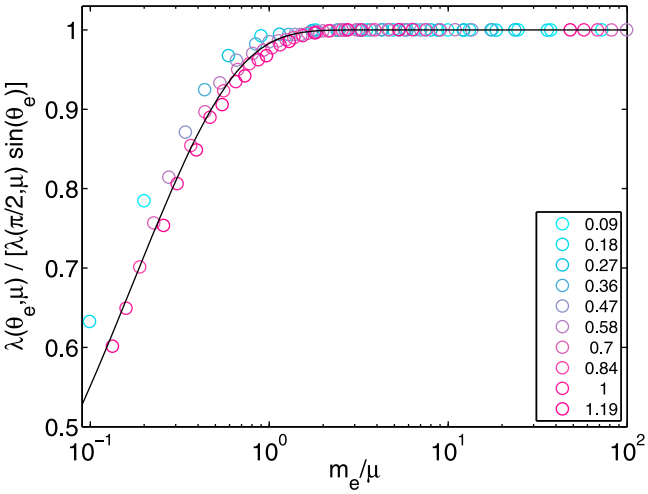

Figure 4. Scaling properties of normalized domain-averaged direct beam radiation for different values of μ (see legend). The empirical fit (black line) yields the scaling function equation (29) which embodies the effect of partial shading for low Sun elevations and the associated reduction of the domain-averaged direct beam flux.

which have been independently obtained from equation (17). The perfect agreement of both curves for $\theta_e = \pi/2 = 90°$ provides some confidence for the correctness of the method.

[24] To derive a simple fit formula, we investigate the scaling of $\overline{\lambda}(\theta_e, \mu)$, normalized by their known values $\overline{\lambda}(\pi/2, \mu)$ and $\overline{\lambda}(\theta_e, 0) = \sin(\theta_e)$. This normalized domain-averaged direct beam component is shown in Figure 4 as a function of the scaling variable m_e/μ. The curves essentially collapse on a single master curve if plotted over m_e/μ, This scaling implies a representation

$$\overline{\lambda}(\theta_e, \mu) = \Lambda(m_e/\mu)\ \sin(\theta_e)\overline{\lambda}(\pi/2, \mu). \tag{28}$$

Here, the scaling function $\Lambda(m_e/\mu)$ captures the reduction of the domain-averaged direct beam radiation for low Sun elevations due to partial shading of the terrain: For $m_e/\mu \gg 1$ $\Lambda(m_e/\mu) \to 1$ and shading is irrelevant. Only if $m_e/\mu \approx 1$, i.e., if the Sun angle attains similar values as the mean slope angle shading becomes relevant and $\Lambda(m_e/\mu) \to 0$ for $m_e/\mu \approx 0$ (sunset). The emergence of the scaling variable m_e/μ implies that the absolute value of the Sun elevation is not meaningful unless given in reference to the terrain slope. This scaling variable has also been used by *Essery and Marks* [2007] to compute the terrain fraction which is self-shaded. The inclusion of partial shading is, e.g., missing in the parametrization [*Dubayah et al.*, 1990].

[25] The scaling function can be reasonably well fitted to

$$\Lambda(x) = \mathrm{erf}[(x/l)^a] \tag{29}$$

with $l = 0.3498$ and $a = 0.4980$ (see black line in Figure 4). The fit function yields $\Lambda(x) \to 0$ for $x \to 0$ and $\Lambda(x) \to 1$ for $x \to \infty$. Together with $\lim_{\mu \to 0} \overline{\lambda}(\pi/2, \mu) = 1$ which follows from equation (17) the parametrization (28) has the correct behavior $\overline{\lambda}(\theta_e, 0) = \sin(\theta_e)$ for $\mu \to 0$ where the parametrization must approach the limit of flat terrain.

3.2. Domain-Averaged Sky View Factor

[26] Next we consider the domain-averaged sky view factor (see Figure 5). It can be very well fitted to

$$\overline{F}_{\mathrm{sky}}(\mu) = \frac{1}{(1 + B\mu^b)^c} \tag{30}$$

with $B = 4.4651$, $b = 2.0083$, $c = 0.2312$.

[27] Since $\overline{F}_{\mathrm{sky}}(\mu)$ and $\overline{\lambda}(\theta_e, \mu)$ fully determine the domain-averaged direct beam, diffuse and terrain radiation, equations (28), (29), and (30) constitute a full subgrid parametrization scheme for the fluxes which includes first-order terrain reflections and partial terrain shading in terms of the Sun elevation θ_e and the terrain parameter μ.

3.3. Effective Albedo for Large-Scale Model Applications

[28] For demonstration purposes we focus on the impact of the subgrid parametrization scheme on the effective albedo which contains all flux components. To this end we apply equation (22) with the derived fits (28), (29), and (30) to the entire Swiss Alps. We start from a high-resolution DHM of Switzerland (Swisstopo) with fine grid size $\Delta x = 25$ m with 15441×9121 grid cells and compute a low-resolution DHM of coarse grid size $L = 5$ km by spatial averaging (nonoverlapping moving window; see Figure 6a). The coarse grid size $L = 5$ km is motivated by the order of present resolutions of regional climate and meteorological models. Note that equation (22) was derived for a single grid cell $\widetilde{A}$ on the coarse grid with vanishing slope. For a fixed Sun position local Sun angles on the coarse grid depend on the mean surface normal vector $\overline{\boldsymbol{n}}$ which varies from cell to cell. Local Sun angles are computed from $\theta_e = \pi/2 - \mathrm{acos}(\overline{\boldsymbol{n}} \cdot \boldsymbol{r}_s)$. The terrain parameter μ is determined by $\mu = \left[\left(\overline{m_x^2 + m_y^2}\right)/2\right]^{1/2}$ and partial height derivatives m_x, m_y are computed from finite (forward) differences from the DHM. The parameter μ is shown in Figure 6b. We have also computed the height variance σ which allows us give a rough estimate of the correlation length via $\xi = \sqrt{2}\sigma/\mu$ (see equation (3) and thereafter). The average correlation length over entire Switzerland is found to be $\xi =$ 866 m leading to $L/\xi \approx 5.77$. Individual values vary between

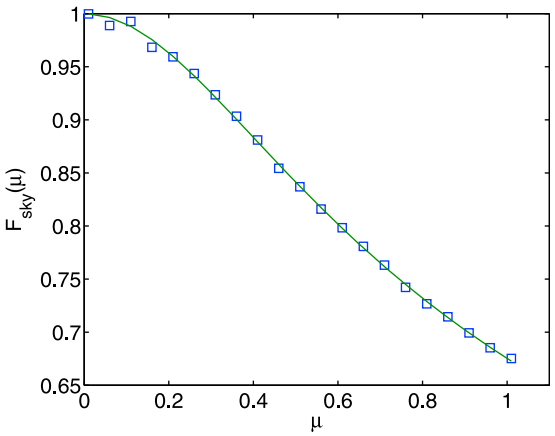

Figure 5. Domain-averaged sky view factor as a function of the terrain parameter μ and the empirical fit from equation (30).

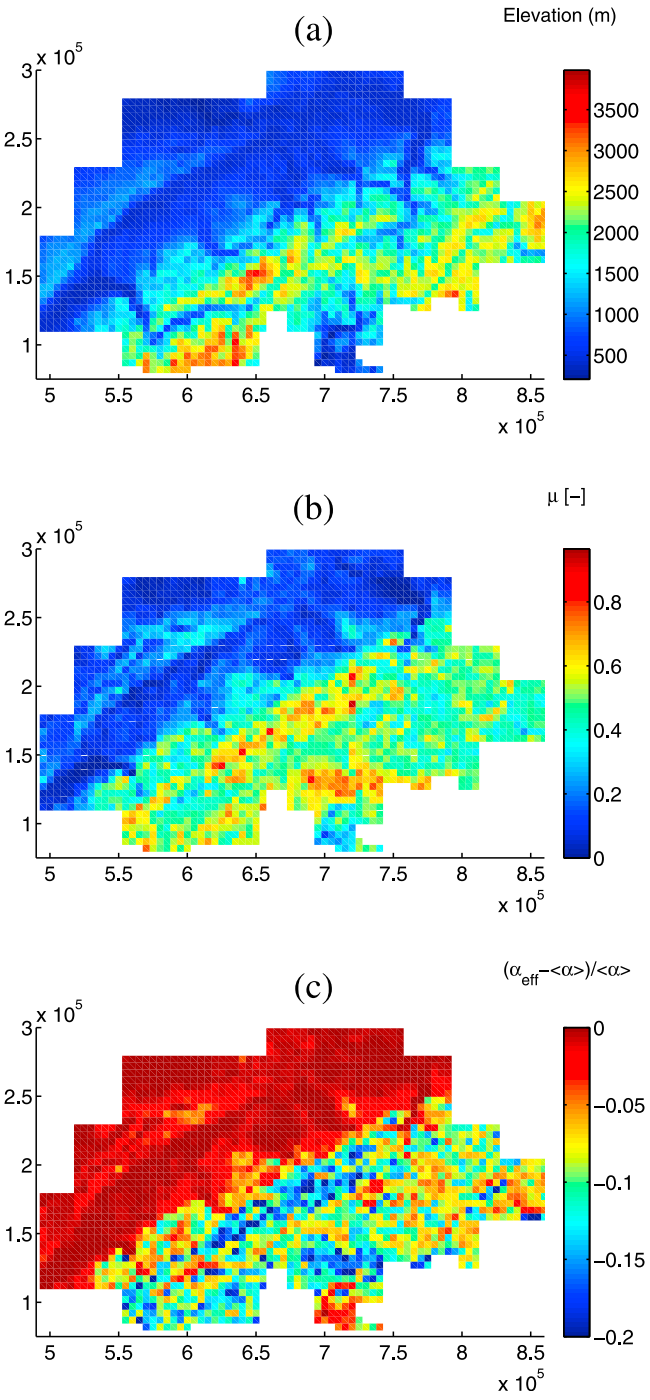

Figure 6. (a) DHM of Switzerland (in Swiss coordinates) with coarse grid size $L = 5$ km obtained from a high-resolution DHM with fine grid size $\Delta x = 25$ m. (b) Terrain parameter μ. (c) Normalized difference of the effective albedo and area-averaged albedo $(\alpha_{\text{eff}} - \langle\alpha\rangle)/\langle\alpha\rangle$ as obtained from equation (22).

the minimum of 92 m and the maximum 2200 m. We thereby confirmed that always $L/\xi > 1$. For the effective albedo we use a Sun elevation of 20° with azimuth in south direction which is typical for the Swiss Alps at noon in December. The azimuth angle enters the computation of the local incidence angles mentioned before. To mimic a partly snow-covered state we assume a relatively high value for the area-averaged albedo of $\langle\alpha\rangle = 0.7$ for all cells on the coarse grid. The direct-to-diffuse ratio was arbitrarily set to $\rho = 10$ which was also used for previous simulations [*Helbig et al.*, 2009] to mimic clear sky conditions over mountains. The relative error between area-averaged albedo and effective albedo is shown in Figure 6c. The average over entire Switzerland is −5.8%. We note that the distribution of errors in Figure 6c, just as the distribution of terrain parameters μ in Figure 6b is bimodal (not shown), reflecting the differences between the Alps and Midlands/Jura. Spatial patterns of the albedo error in Figure 6c inherit some spatial characteristics of the slope parameter μ in Figure 6b via equation (22). In turn, μ inherits characteristics of the underlying relief: The belt of enhanced μ around position (710000, 130000) in Figure 6b, which is not signaled by the elevation model in Figure 6a, is known as the Lepontine-Bergell area with increased averaged slope characteristics [*Kuhni and Pfiffner*, 2001]. We have repeated the analysis also for a coarser resolution of $L = 10$ km (not shown). The results are consistent with those obtained for $L = 5$ km and yield spatial distributions very similar to those in Figures 6b and 6c. The relative errors between area-averaged albedo and effective albedo obtained here are in the same order of magnitude as those obtained by *Weihs et al.* [2000] for UV radiation in the Sonnblick region, Austria. It is noteworthy that the entire processing leading to Figure 6 takes less than a minute on a 2.8 GHz AMD Opteron.

4. Discussion and Conclusions

[29] We have shown that the radiosity equation on Gaussian random fields provides a theoretical framework in which spatially averaged radiation transfer can be treated analytically to a large extent. The elaborate derivation via the level-crossing probability has been shown to be useful to derive formally exact expressions for all radiation quantities and the sky view factor. Derived equations enable robust empirical fits for a wide range of parameter values which can be easily applied to compute effective albedos.

[30] As noted by *Essery and Marks* [2007] the nonlocal horizon and thereby the radiation fluxes in complex terrain are extreme-value properties of the topography. Horizon statistics can thus be expected to show some degree of universality and robustness against changes in the underlying topography model. Therefore we do not expect the assumption of Gaussian topographies to be very restrictive. In addition, we have shown that some aspects of real topography on length scales 2.5 km < L < 6.5 km are reasonably well captured by Gaussian statistics [*Helbig and Löwe*, 2012].

[31] We only focused on the simplest mathematical setup to demonstrate the utilization of the level-crossing probability. Regarded as a reference to guide parametrizations, the method is amenable to generalizations if limitations can be identified quantitatively, e.g., by Monte Carlo simulations [*Lee et al.*, 2011] of radiation transfer on Gaussian random fields as an idealized topography model. We have not touched the issue of grid resolution here. The covariance (2) leads to differentiable realizations of the field [*Adler*, 1981] and, in turn, to a slope distribution (3) as an inherent property of the topography which is not affected by DHM resolution. If the grid size of the fine grid $\Delta x \ll \xi$

is chosen sufficiently small compared to the correlation length ξ the influence of grid resolution is negligible [see also *Helbig et al.*, 2009]. This seems to be justified for the present application of the theory to Switzerland with Δx = 25 m and our estimate ξ = 866 m for the average correlation length. A DHM resolution of 20–30 m was also recommended by *Arnold and Rees* [2009] within a distributed, parametrized radiation model based on sky view factor calculations for an arctic valley glacier. The effect of DHM resolution was also addressed by *Weihs et al.* [2012] within a 3-D Monte Carlo simulation for UV radiation in the Sonnblick and Innsbruck area in Austria. The smallest grid size considered in the latter study was Δx = 50 m, however no reference to a lateral correlation length was made therein. In general, an impact of DHM resolution is common to all approaches to ground-based radiation in complex terrain if the topography is insufficiently resolved by the DHM. Note that the impact of fine grid size Δx has to be contrasted to the impact of coarse grid size L of the large-scale model. The latter must be chosen sufficiently *large* compared to the correlation length, i.e., $L \gg \xi$, to be consistent with our assumptions.

[32] In the following we discuss available generalizations of our methodology which have been treated in the original work along the lines of scattering from rough surfaces.

[33] 1. Natural mountains might be anisotropic due to larger-scale valleys. Anisotropic topographies can be treated within the full two-dimensional approach of surface shadowing treated in *Bourlier and Berginc* [2003]. Technically, this requires replacement of $p(m_h|m_x)$ by $p(m_h|m_x, m_y)$ in equation (24). However, we believe that anisotropy is of minor importance if the coarse grid size is sufficiently large, as previously shown in *Helbig and Löwe* [2012].

[34] 2. In the present work we assumed that $L/\xi \gg 1$ such that emerging area averages can be computed from ensemble averages. This is not necessarily the case depending on the coarse grid resolution L and the correlation length ξ. For our application we found an average of $L/\xi \approx 5.77$ over all of Switzerland which appears to be not very large. As in our case, applications generally use DHMs with fixed coarse-resolution L. Thereby every grid cell contains a different subgrid topography and thus different correlation lengths ξ. This leads to position-dependent corrections since ratios of L/ξ differ from cell to cell. In the present framework the order of magnitude of such corrections can be addressed from the level-crossing probability with limited "observation length" as computed in *Bourlier et al.* [2002]. The order of magnitude of the corrections for finite L/ξ deserves further attention and will be addressed in future work.

[35] 3. Here we focused on the case where the bare albedo $\alpha(\boldsymbol{x})$ is independent of the topography. In view of climatological applications, e.g., for coupling a radiation balance to subgrid snow line dynamics, it seems necessary to incorporate an elevation dependence $\alpha = \alpha(h(\boldsymbol{x}))$ which allows representation of a snow line separating high-albedo (snow-covered) regions above the snow line and low-albedo regions (trees, bare rock, etc.) below the snow line. Such a scenario was also considered by *Weihs et al.* [2000, 2001] for UV radiation. This general case of a slope- and elevation-dependent albedo $\alpha = \alpha(h, m_x, m_y)$ requires conditioning the level-crossing probability $p(m_h|m_x, m_y)$ in equation (20) not only on the slope m_x, m_y, but also on the elevation $p(m_h|m_x, m_y, h)$. This generalization can also be treated within the framework of level-crossing probability and has already been treated in *Wagner* [1967], *Bourlier et al.* [2002], and *Bourlier and Berginc* [2003]. The same methodology applies to tackling potential elevation dependencies of the bare fluxes such as an altitude dependence of the diffuse flux mentioned in *Lee et al.* [2011].

[36] 4. The bidirectional case of the level-crossing problem (required for remote sensing applications) is also addressed in *Wagner* [1967], *Bourlier et al.* [2002], and *Bourlier and Berginc* [2003].

[37] Though limited to clear sky conditions we believe that our results provide a constructive first-order estimate of shortwave fluxes in complex terrain, which can be readily generalized if particular assumptions have proven wrong. Analytical results will certainly gain importance if the energy balance in complex terrain is coupled to the mass balance of snow and ice. This interaction is crucial as long as climate change is assessed from the state of the cryosphere which severely demands minimal models with known limitations.

[38] **Acknowledgments.** The authors thank Richard Essery and two anonymous reviewers for helpful comments on the manuscript. N. Helbig was supported by an individual fellowship of the Swiss National Science Foundation (grant PBZHP2-131044). Part of the work was done with financial support from the European Commission (AWARE project, contract SST4-CT-2004-012257).

References

Adler, R. (1981), *The Geometry of Random Fields*, John Wiley, London.

Arnold, N., and G. Rees (2009), Effects of digital elevation model spatial resolution on distributed calculations of solar radiation loading on a High Arctic glacier, *J. Glaciol.*, *55*, 973–984.

Atkinson, K. (2006), A study of the fast solution of the occluded radiosity equation, *Electron. Trans. Numer. Anal.*, *23*, 219–250.

Bourlier, C., and G. Berginc (2003), Shadowing function with single reflection from anisotropic Gaussian rough surface: Application to Gaussian, Lorentzian and sea correlations, *Waves Random Media*, *13*, 27–58.

Bourlier, C., G. Berginc, and J. Saillard (2002), Monostatic and bistatic statistical shadowing functions from a one-dimensional stationary randomly rough surface according to the observation length: I. Single scattering., *Waves Random Media*, *12*, 145–173.

Chen, Y., A. Hall, and K. Liou (2006), Application of three-dimensional solar radiative transfer to mountains, *J. Geophys. Res.*, *111*, D21111, doi:10.1029/2006JD007163.

Dozier, J., and J. Frew (1990), Rapid calculation of terrain parameters for radiation modeling from digital elevation data, *IEEE Trans. Geosci. Remote Sens.*, *28*, 963–969.

Dozier, J., and S. I. Outcalt (1979), An approach toward energy-balance simulation over rugged terrain, *Geogr. Anal.*, *11*, 65–85.

Dubayah, R., J. Dozier, and F. W. Davis (1990), Topographic distribution of clear-sky radiation over the Konza Prairie, Kansas, *Water Resour. Res.*, *26*, 679–690, doi:10.1029/WR026i004p00679.

Essery, R., and D. Marks (2007), Scaling and parametrization of clear-sky solar radiation over complex topography, *J. Geophys. Res.*, *112*, D10122, doi:10.1029/2006JD007650.

Gradshteyn, I. S., and I. M. Ryzhik (2000), *Tables of Integrals, Series, and Products*, 6th ed., Academic, San Diego, Calif.

Helbig, N., and H. Löwe (2012), Shortwave radiation parameterization scheme for subgrid topography, *J. Geophys. Res.*, *117*, D03112, doi:10.1029/2011JD016465.

Helbig, N., H. Löwe, and M. Lehning (2009), Radiosity approach for the surface radiation balance in complex terrain, *J. Atmos. Sci.*, *66*, 2900–2912.

Helbig, N., H. Löwe, B. Mayer, and M. Lehning (2010), Explicit validation of a surface shortwave radiation balance model over snow-covered complex terrain, *J. Geophys. Res.*, *115*, D18113, doi:10.1029/2010JD013970.

Kuhni, A., and O. Pfiffner (2001), The relief of the Swiss Alps and adjacent areas and its relation to lithology and structure: Topographic analysis from a 250-m DEM, *Geomorphology*, *41*, 285–307.

Lee, W.-L., K. N. Liou, and A. Hall (2011), Parameterization of solar fluxes over mountain surfaces for application to climate models, *J. Geophys. Res.*, *116*, D01101, doi:10.1029/2010JD014722.

Liou, K. N., W.-L. Lee, and A. Hall (2007), Radiative transfer in mountains: Application to the Tibetan Plateau, *Geophys. Res. Lett.*, *34*, L23809, doi:10.1029/2007GL031762.

Manners, J., S. B. Vosper, and N. Roberts (2012), Radiative transfer over resolved topographic features for high-resolution weather prediction, *Q. J. R. Meteorol. Soc.*, *138*, 720–733.

Marshak, A., and A. Davis (Eds.) (2005), *3D Radiative Transfer in Cloudy Atmospheres*, Springer, Berlin.

Müller, M. D., and D. Scherer (2005), A grid- and subgrid-scale radiation parameterization of topographic effects for mesoscale weather forecast models, *Mon. Weather Rev.*, *133*, 1431–1442.

Olyphant, G. A. (1986), The components of incoming radiation within a mid-latitude alpine watershed during the snowmelt season, *Arct. Alp. Res.*, *18*, 163–169.

Parajka, J., S. Dadson, T. Lafon, and R. Essery (2010), Evaluation of snow cover and depth simulated by a land surface model using detailed regional snow observations from Austria, *J. Geophys. Res.*, *115*, D24117, doi:10.1029/2010JD014086.

Schmucki, D., S. Voigt, R. Phillipona, C. Fröhlich, J. Lenoble, A. Ohmura, and C. Wehrli (2001), Effective albedo derived from UV measurements in the Swiss Alps, *J. Geophys. Res.*, *106*(D6), 5369–5383, doi:10.1029/2000JD900712.

Wagner, R. J. (1967), Shadowing of randomly rough surfaces, *J. Acoust. Soc. Am.*, *41*, 138–147.

Weihs, P., H. Scheifinger, G. Rengarajan, and S. Simic (2000), Effect of topography on average surface albedo in the ultraviolet wavelength range, *Appl. Opt.*, *39*, 3592–3603.

Weihs, P., et al. (2001), Modeling the effect of an inhomogeneous surface albedo on incident UV radiation in mountainous terrain: Determination of an effective surface albedo, *Geophys. Res. Lett.*, *28*(16), 3111–3114.

Weihs, P., et al. (2012), The influence of the spatial resolution of topographic input data on the accuracy of 3-D UV actinic flux and irradiance calculations, *Atmos. Chem. Phys.*, *12*(5), 2297–2312.

Wen, J., Q. Liu, Q. Liu, Q. Xiao, and X. Li (2009), Scale effect and scale correction of land-surface albedo in rugged terrain, *Int. J. Remote Sens.*, *30*, 5397–5420.